*Bull. Mater. Sci.* (2022)45:12
https://doi.org/10.1007/s12034-021-02591-3



# Improvement of hydriding kinetics of $LaNi_5$-type metal alloy through substitution of nickel with tin followed by palladium deposition

**THABANG R SOMO[1,2], KWENA D MODIBANE[1,*], MOEGAMAT W DAVIDS[2], MYKHAYLO V LOTOTSKYY[2] and MPITLOANE J HATO[1]**

[1]Nanotechnology Research Group, Department of Chemistry, School of Physical and Mineral Sciences, University of Limpopo (Turfloop), Polokwane 0727, South Africa

[2]HySA System, South African Institute for Advanced Material Chemistry, University of the Western Cape, Cape Town 7535, South Africa

*Author for correspondence (kwena.modibane@ul.ac.za)

MS received 29 October 2020; accepted 6 April 2021

**Abstract.** Hydrogen absorption performances of $LaNi_5$ alloy are sensitive to the surface reactions with poisonous gases, such as oxygen, readily forming oxides/hydroxides. In this study, we report the studies on the hydrogen absorption behaviour of $AB_5$-type hydrogen storage alloys, formed by $LaNi_{(5-x)}Sn_x$ ($X = 0.2$) followed by electroless Pd deposition. The uncoated and Pd-coated materials were characterized using scanning electron microscopy/energy dispersive spectroscopy (SEM/EDS), atomic absorption spectroscopy (AAS), X-ray diffraction (XRD) and Brunauer–Emmet–Teller. XRD analyses indicated that both $LaNi_5$ and $LaNi_{4.8}Sn_{0.2}$ alloys crystallize in $CaCu_5$-type crystal structure, while SEM analysis and particle size distribution histograms showed increment in particle size upon Sn incorporation. Palladium particles on the surface of the materials were detected by AAS and EDS analyses. Furthermore, substitution of a small fraction of Ni by Sn leads to an increase in hydrogen absorption capacity even without activation. Moreover, a decrease in hydrogen absorption rate was observed for $LaNi_{4.8}Sn_{0.2}$ alloy and this was related to an increment in the crystalline unit cell volume. Kinetic curves of Pd-coated alloys show superior absorption kinetics compared to their uncoated counterparts due to high affinity of Pd for hydrogen.

**Keywords.** Hydrogen storage materials; energy storage materials; $AB_5$ alloy; palladium deposition.

## 1. Introduction

Hydrogen gas plays an important role in reduction of carbon dioxide to hydrocarbons [1]. However, lack of feasible methods to store hydrogen in a safe and compact way is one of the main drawbacks in hydrogen technology [2]. So far, hydrogen compression is considered the simplest and most convenient method of hydrogen storage. This is confirmed by commercial hydrogen vehicle manufacturers, who utilize only high-pressure hydrogen tanks. Nevertheless, more energy associated with hydrogen compression is not economically favoured [3]. The most promising way is to store hydrogen in solid absorbents, such as metal alloys in which hydrogen bound to these materials to form metal hydrides [4]. An attractive feature of solid-state storage is that the absorption of hydrogen using many of these metal alloy materials is reversible, thereby reducing operational costs [5]. The most interesting class of hydride-forming materials is the $AB_5$-type metal hydride material due to its advantages, such as easy activation, moderate plateau pressure and high hydrogen capacity at room temperature [5]. For example, inactivated $LaNi_5H_6$ has a volumetric capacity of $5.5 \times 10^{22}$ atoms $cm^{-3}$ and gravimetric capacity of 1.4 wt% at ambient temperature [6]. However, the difficulties in initial activation and slow hydriding/dehydriding kinetics at ambient conditions (room temperature and 1013.25 mbar) are among the drawbacks that prohibit the use of the $AB_5$ materials as hydrogen sorbents [7]. Additionally, easy and quick degradation and poisoning intolerance of neat $AB_5$ alloy during hydrogenation/dehydrogenation is also a major disadvantage of the material [5]. For instance, the poisoning tolerance of a typical $AB_5$ alloy was tested in the study by Modibane *et al* [8]. In that study we observed that during the hydrogen separation from $CO_2$/CO containing gas mixtures over the $AB_5$ materials ($La(Ni,Co,Mn,Al)_5$ substrate), the amount of hydrogen being separated from the gas mixture is lower at equivalent gas concentrations than when poisonous gases are in small amounts. This observation is a clear indication that the amount of hydrogen absorbed on an alloy material

Published online: 29 December 2021

and the adsorption rate are more dependent on the purity of the alloy surface. Methods such as spark plasma sintering [9], mechanical alloying [10], melt spinning [11], high hydrogen pressure method [12], hydriding combustion synthesis [13], surface modification (such as autocatalytic deposition of palladium) [13,14] and alloying with other elements (substitution of B-component in $AB_5$) [15,16] have been widely studied for improvement of hydrogen absorption kinetics of metal hydrides from gas mixture. Our recent findings [17] demonstrated the improvement of poisoning tolerance and hydrogen absorption using palladium black addition on $AB_5$ alloy followed by electroless Pd deposition. The combination of partial substitution of Ni and Pd deposition is extremely active towards dissociative hydrogen chemisorption and permeable for hydrogen atoms, which enable hydrogen to rapidly adsorb onto the bulk material while still maintaining the hydrogenation activity even after exposure to poisonous gaseous environment [18]. Recently, Hubkowska *et al* [19] examined the electrochemical behaviour of an $AB_5$ alloy powder coated with Pd nanoparticles (ca. 3.5 wt%) obtained by microwave-assisted polyol synthesis. The authors found that the microwave-assisted polyol method makes it possible to obtain Pd nanoparticles of irregular shapes and sizes, unevenly distributed on the $AB_5$ surface allowing fast kinetics of hydrogen absorption/desorption processes. However, microwave-assisted polyol method requires large amount of palladium (usually >3.5 wt%), which is not economical and cost effective. Another interesting deposition technique is electroless (autocatalytic) plating method, and an average 0.5 wt% of palladium nanoparticles can be deposited through this technique [20]. In addition, autocatalytic deposition of palladium can also result in improvement of surface catalytic activity, specific surface area layer, activation characteristics as well as protective nature of metal hydrides against poisoning materials [21]. Due to the inclusion of phosphorus into the metal coating, the amorphous nature of the palladium coating may also improve the hydrogen capacity of the materials, as it is documented that amorphous materials can take and release large amount of hydrogen compared to their polycrystalline counterparts [20]. Phosphorous is impregnated into the Pd layer and promotes the formation of amorphous electroless-deposited metal coatings [20,22]. Therefore, this study reports on the effects of partial substitution of Ni by Sn in $LaNi_5$ alloy followed by autocatalytic deposition of Pd on hydrogen adsorption capacity and kinetics. These $AB_5$ alloys containing nickel are also widely used in hydride (Ni-MH) batteries [5]. Tin is also known to enhance the cycling stability of $LaNi_5$ alloy, as it has advanced electron attractive power and bigger active sites than that of nickel. Similar results were reported by Ishibashi *et al* [23]. Combining the merits of Ni(Sn) in $LaNi_{4.8}Sn_{0.2}$ alloy and poisoning tolerance of Pd-coated alloy, Pd-coated $LaNi_{4.8}Sn_{0.2}$ alloy was prepared in this contribution through simple arc melting method followed by autocatalytic Pd plating. This study can provide further insights into the properties of metal hydride hydrogen storage material after pre-exposure to air. To our knowledge, the preparation of Pd-$LaNi_{4.8}Sn_{0.2}$ alloy for hydrogen absorption kinetics has not been reported to date. In this study, we show significant activity in hydrogen absorption kinetics after pre-exposure to air as compared to unmodified $LaNi_5$ alloy.

## 2. Experimental

### 2.1 *Materials*

The $AB_5$-type ($LaNi_5$ and $LaNi_{4.8}Sn_{0.2}$) hydride-forming alloys were prepared from La (99.9%), Ni (99.95%) and Sn (99.98%), purchased from Sigma Aldrich. The $AB_5$ hydride-forming alloy was prepared by arc-melting on a water-cooled copper crucible in protective argon atmosphere. All prepared ingots were melted three times to provide homogeneity. Subsequently, the prepared metal ingots were pulverized by ball-milling in argon for 10 min. The materials were allowed to constant exposure to air throughout the experimental studies.

### 2.2 *Surface modification of alloy*

Surface modification of the substrate materials was conducted through autocatalytic deposition of Pd in hypophosphite-based bath, following a procedure described by Denys *et al* [20]. The rationale behind this approach was the combination of the enhanced activation kinetics observed with deposition of Pd catalytic layers and to form materials with excellent hydrogen sorption properties. The autocatalytic deposition of Pd was applied to $\sim$5 g batch of each substrate ($LaNi_5$ and $LaNi_{4.8}Sn_{0.2}$ alloys). Prior to palladium deposition, the materials were first sensitized and activated in a palladium–tin (Pd–Sn) colloidal solution [20], resulting in increased densities of Pd deposition and surface Pd loading on the intermetallide.

### 2.3 *Characterization techniques*

X-ray diffraction (XRD) studies of the alloys were performed using a Bruker Advance powder diffractometer (Madison, USA; 40 mA, 40 keV, $\lambda$Cu-K = 0.15406 nm) at the Materials Research Group, iThemba Labs, in Cape Town, South Africa, for phase identification. Scanning electron microscopes/energy-dispersive spectroscopy (SEM/EDS, Edax Genesis, 100 live seconds) studies were carried out using Leo 1450 microscope (20 kV, secondary electrons) at the Physics Department, University of the Western Cape (UWC), to evaluate the morphology of $AB_5$-type alloy particle size/shape; Pd particle dispersion on the surface of the $AB_5$-type alloy particles and Pd particle size/

shape. The elemental analysis was determined using a Perkin Elmer AAnalyst 400 atomic absorption spectrometer (AAS) to ascertain the quantity of palladium deposited on the surface of the materials. A Tristar micromeritics instrument was used for low-pressure nitrogen (77 K) adsorption/desorption isotherms, Brunauer–Emmet–Teller (BET) surface area and pore volume measurements. Approximately 0.5 g of alloy was de-gassed by heating at 180°C under $N_2$ flow for 24 h. The BET measurements were used to evaluate the effect of Pd deposition on the surface area and pore volume of the parent $AB_5$ materials.

The effect of partial substitution of nickel by tin followed by autocatalytic palladium deposition on the kinetics of hydrogen absorption was studied. In addition, a comparison of hydrogen absorption before (after pre-exposure to air) and after activation by evacuation and heating at 300°C was done. Evacuation and heating prevented the possibility of the presence of residual oxygen on the surface of the alloy. Hydrogen absorption was conducted using a Sieverts-type volumetric installation, South African Institute for Advanced Material Chemistry (SAIAMC), UWC. The measurements were carried out at $T = 20°C$, $P_0 \sim 30$ bar $H_2$, for 2 h. The experimental results were processed by application of formal kinetic analysis, using the Avrami–Erofeev equation (1) [17]:

$$\left(\frac{H}{\mathrm{AB5}}\right) = \left(\frac{H}{\mathrm{AB5}}\right)_{\max} - \left\{1 - \exp\left(-\left(\frac{t}{t_0}\right)^n\right)\right\}, \qquad (1)$$

where $(H/AB_5)$ is the actual hydrogen concentration in the alloy; $(H/AB_5)_{max}$ is the maximum hydrogen concentration in the alloy; $t$ is time; $t_0$ the characteristic time of hydrogen absorption (reciprocal rate constant k); and the index of power, $n$, is interpreted as a value indirectly connected to the reaction mechanism.

## 3. Results and discussion

### 3.1 *Structural characterization*

The ball-cast $LaNi_5$ alloy (figure 1a) is comprised of a single $CaCu_5$-type phase with lattice periods ($a$ = 5.0285 Å and $c$ = 3.9931 Å), corresponding well to the literature data for the same material derived from synchrotron XRD measurements [24]. After partial substitution of Sn for Ni in $LaNi_5$ alloy (figure 1b and table 1), a one-phase structure that is composed of major $CaCu_5$-type intermetallic phase with lattice parameters $a$ = 5.0652(3) Å and $c$ = 4.0326(2) Å is observed. Furthermore, the pattern of Sn-substituted material consists of broadened diffraction peaks as compared to $LaNi_5$ material and the peaks have shifted towards lower $2\theta$ values, while their intensities weakened. The reduction and shift of diffraction peaks (as illustrated in figure 1b), imply an increase in the lattice parameters (table 1) with partial replacement of Ni by Sn in the $AB_5$ alloys [13]. All these effects are attributed to inhomogeneity in the B-component (Ni(Sn)) of the parent $AB_5$-type material [20] and the larger Van der Waals radius (224 pm) of Sn compared to the radius of Ni (200 pm). In addition, the crystallite sizes were calculated from the Scherrer formula (equation 2) and represented in table 1.

$$\tau = (\kappa\lambda)/\beta\cos(\theta) \qquad (2)$$

Noticeably, the crystallite size decreased from 5.52 nm of $LaNi_5$ to 5.11 nm (table 1), suggesting partial substitution of Ni due to the inclusion of bigger active sites of Ni. This change in crystallite size further support the broadening of the diffraction reflections of the Sn-substituted material as derived from the fact that tin has bigger active sites than that of nickel, allowing lattice expansion [25]. The refinement of the XRD data of $LaNi_{4.8}Sn_{0.2}$ alloy showed an increase in the unit cell volume and lattice constants. The estimated abundance and lattice period of this phase exhibit a trend of increase with introduction of Sn in the charge (table 1). This observation allows us to suggest that Sn (structure type Cu, $a$ = 5.0652(3) Å and $c$ = 4.0326(2) Å) substitutes Ni in the Ni-based phase further referred as Ni(Sn). The Sn content in Ni(Sn) estimated from its lattice period by applying Vegard's law [17] (shown in the last column of table 1) was around 0.724%. This shows the formation of a small amount of orthorhombic Ni(Sn) phase, which agrees with the previous report [23]. Interestingly, the unit cell aspect ratio ($c/a$) for the $AB_5$ phase slightly increased after partial substitution of Ni by Sn from 0.794 to 0.796 (or by 0.25%).

On the other hand, the XRD patterns of $LaNi_5$ (figure 1c) and $LaNi_{4.8}Sn_{0.2}$ (figure 1d) materials after autocatalytic Pd deposition revealed sharp diffraction peaks, which are in resemblance with the diffraction peaks of Pd-uncoated alloys. The Pd-$LaNi_5$ and Pd-$LaNi_{4.8}Sn_{0.2}$ alloys crystallized in the hexagonal $CaCu_5$-type structure with lattice parameters $a$ = 5.0285(2) Å, $c$ = 3.9931(2) Å and a crystallite size of 5.52 nm; and $a$ = 5.0583(3) Å, $c$ = 4.0229(4) Å and a crystallite size of 5.09 nm, respectively, as presented in table 1. After Pd deposition, the Sn content in Ni(Sn) estimated from its lattice period by applying Vegard's law (table 1) decreased to 0.589%. Moreover, palladium is not expected to get incorporated in the $AB_5$ materials either substitutionally or interstitially [20]. Hence, there are no noticeable changes in either broadness or position of diffraction peaks after surface modification. The X-ray diffractograms of Pd-modified materials do not show any palladium phase. The absence of palladium phase may be due to the amorphous nature of the particles from electroless plating bath or the lack of detectable quantities for XRD analysis [4]. It was seen that after Pd deposition, there was a slight decrease of $c/a$ and unit cell volume for the $AB_5$ phase due to low surface loadings of the Pd on the surface of the $AB_5$-type intermetallic [4].

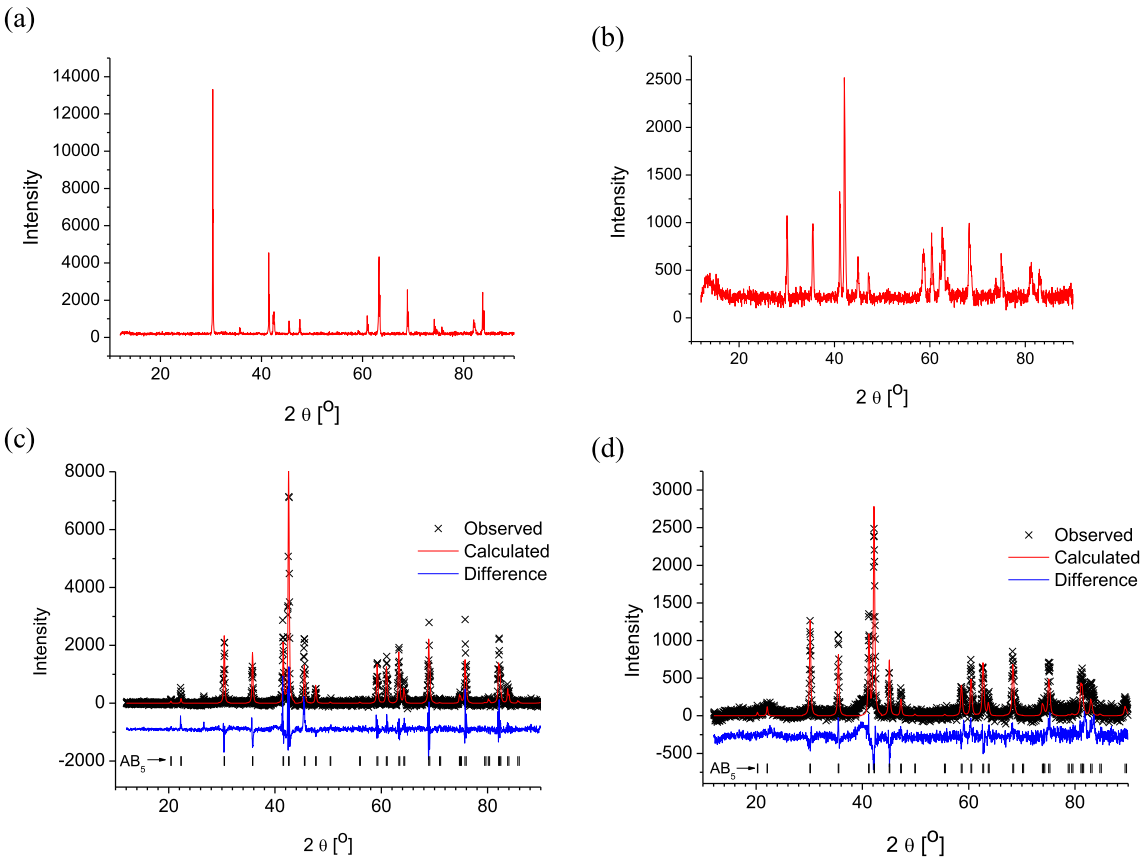


**Figure 1.** X-ray diffractogram of (**a**) as-cast $LaNi_5$, (**b**) as-cast $LaNi_{4.8}Sn_{0.2}$, (**c**) surface-modified Pd-$LaNi_5$ and (**d**) surface-modified Pd-$LaNi_{4.8}Sn_{0.2}$.

**Table 1.** Results of refinement of XRD patterns of $AB_5$-type alloys.

| Sample | Preparation condition | | Lattice constants | | Unit cell volume | Crystallite size | Estimated Sn content in the phase |
|---|---|---|---|---|---|---|---|
| | Sn | Pd | *a* (Å) | *c* (Å) | *V* (Å$^3$) | $\tau$ (nm) | (at%) |
| $LaNi_5$ | No | No | 5.0285(2) | 3.9931(2) | 87.442(8) | 5.52 | — |
| $LaNi_{4.8}Sn_{0.2}$ | Yes | No | 5.0652(3) | 4.0326(2) | 89.601(9) | 5.11 | 0.724(5) |
| Pd-$LaNi_5$ | No | Yes | 5.0188(2) | 3.9823(2) | 86.870(7) | 5.52 | — |
| Pd-$LaNi_{4.8}Sn_{0.2}$ | Yes | Yes | 5.0583(3) | 4.0229(4) | 89.14(1) | 5.09 | 0.589(1) |

### 3.2 *Morphological and elemental characterizations*

The surface morphologies and particle size distribution of the $LaNi_{4.8}Sn_{0.2}$ and $LaNi_5$ alloys are shown in figure 2a–f, respectively. The morphological studies were carried out using high resolution-SEM, which is able to detect nano-sized Pd particles. Figure 2a and b shows that $LaNi_5$ alloy powder is comprised of clean, smooth surface with particles varying in size from 1 to 11 μm, as depicted by particle size distribution histogram (figure 2c). Similar results were reported by Cuevas and Hirscher [14]. From the histogram, it was observed that the majority of the alloy particles have particle size of ∼1 μm. After Sn incorporation, the appearance of large particles ranging at 9–13 μm on the surface of $AB_5$ alloy is observed (figure 2d and e). When comparing particle size distribution histograms (figure 2c and f) of the two alloys, it is seen that the particle sizes changed from a range of 1–8 to 1–14 μm after Sn substitution.

In parallel to these SEM studies, EDS analyses were employed for determination of the elemental compositions of $AB_5$ alloys. The EDS data (table 2) showed a satisfactory

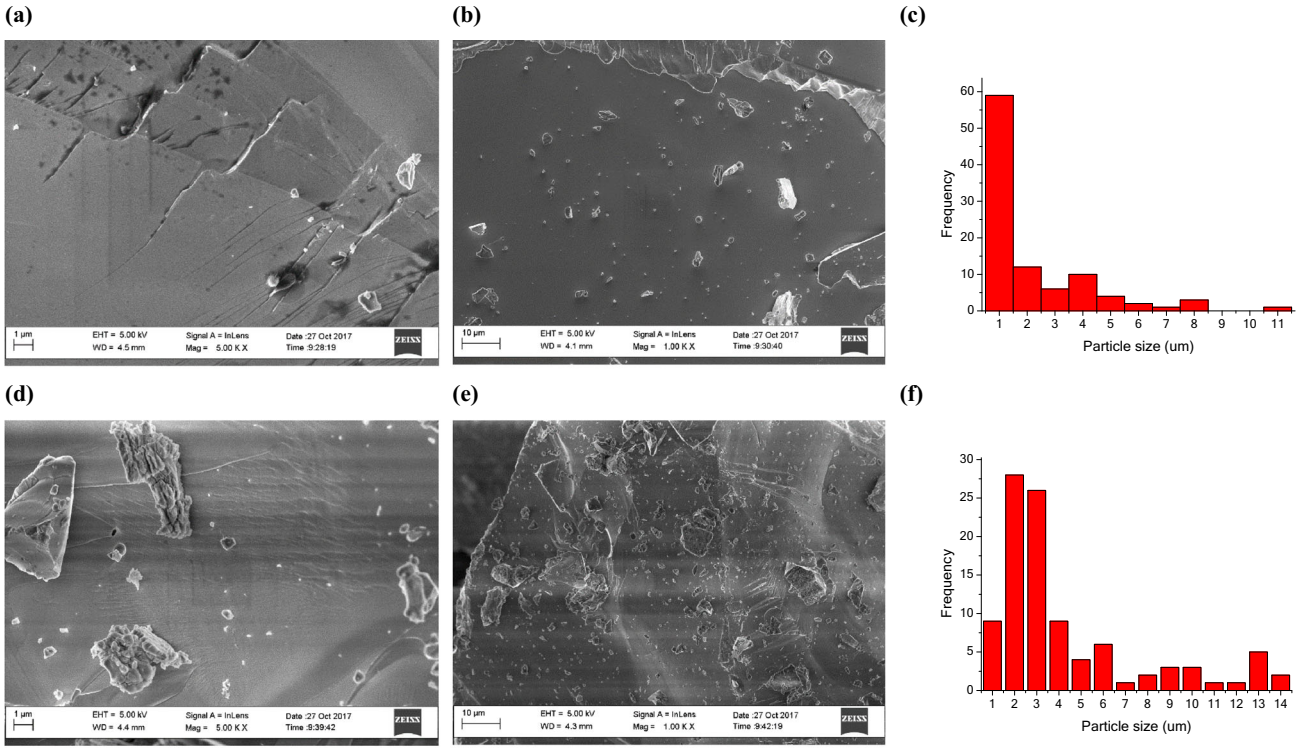


**Figure 2.** SEM micrographs of (**a**, **b**) $LaNi_5$ and (**c**, **d**) $LaNi_{4.8}Sn_{0.2}$ and their particle size distribution histograms ((**c**) Pd-$LaNi_5$ and (**f**) Pd-$LaNi_{4.8}Sn_{0.2}$).

**Table 2.** Elemental composition data of $LaNi_5$ and $LaNi_{4.8}Sn_{0.2}$ alloy.

| Materials | Element | EDS data | | Target composition |
|---|---|---|---|---|
| | | Net counts | Wt% | (Wt%) |
| $LaNi_5$ | La | 7.2 | 33.96 | 32.18 |
| | Ni | 9 | 66.04 | 67.93 |
| | Total | — | 100.00 | 100.00 |
| $LaNi_{4.8}Sn_{0.2}$ | La | 6.6 | 32.92 | 31.31 |
| | Ni | 8.4 | 61.22 | 63.44 |
| | Sn | 3.4 | 5.86 | 5.35 |
| | Total | — | 100.00 | 100.00 |

alignment with a target alloy composition (represented in last columns). From the table, it is observable that the EDS result for $LaNi_{4.8}Sn_{0.2}$ alloy shows some overestimation in Sn content, indicating that slightly more than 0.2 of Sn element was added. Comparison of the fractions of the 'B' components of the $LaNi_{4.8}Sn_{0.2}$ alloy indicated that the alloy is a typical non-stoichiometric alloy with Sn and Ni occupying the 'B' site to form Ni(Sn) [16]. The occurrence of palladium-phosphorus particles on the surfaces of the materials that underwent autocatalytic deposition of Pd was observed on SEM images to be spherical (figure 3a, b, d and e). Palladium coatings on the $AB_5$-type substrates were found to be discontinuous in nature. Similar observations were observed before by Denys *et al* [20]. Furthermore, it was observed on the particle size distribution histograms that the Pd-coated $LaNi_5$ alloy consisted of Pd particles ranging in size between 1 and 36 nm, with majority having particle size of 4 to 7 nm (figure 3c).

Pd-coated $LaNi_{4.8}Sn_{0.2}$ alloy is comprised of Pd particles in the range of 3–17 nm (figure 3f). On a contrary, Denys *et al* [20] observed larger and wider size distribution of 135 nm exhibited by Pd particles on the $AB_5$ alloy. The reason for more homogeneous deposition of Pd on the Sn-substituted alloy can be attributed to more surface roughness of the $LaNi_{4.8}Sn_{0.2}$ alloy due to the addition of Sn within the parent alloy. The surface Pd loading of surface-modified $AB_5$ alloys was estimated using EDS (figure 4c and d). It was observed in the figures that both alloys showed Pd peak at the same intensity. This was supported by very close amounts of Pd deposited for each alloy, recorded by EDS to be 1.35 wt% for Pd-$LaNi_5$ and 1.44 wt% for Pd-$LaNi_{4.8}Sn_{0.2}$ alloy. Some traces of phosphorous, which are due to the presence of phosphorous in $NaH_2PO_2$-based plating bath, were revealed by EDS on the surface of each Pd-coated alloy. In support to EDS analysis, AAS was employed to further ascertain the quantity of palladium deposited on the $AB_5$ alloys. The total deposited Pd determined using AAS was found to be 0.1044 wt% for both modified alloys.

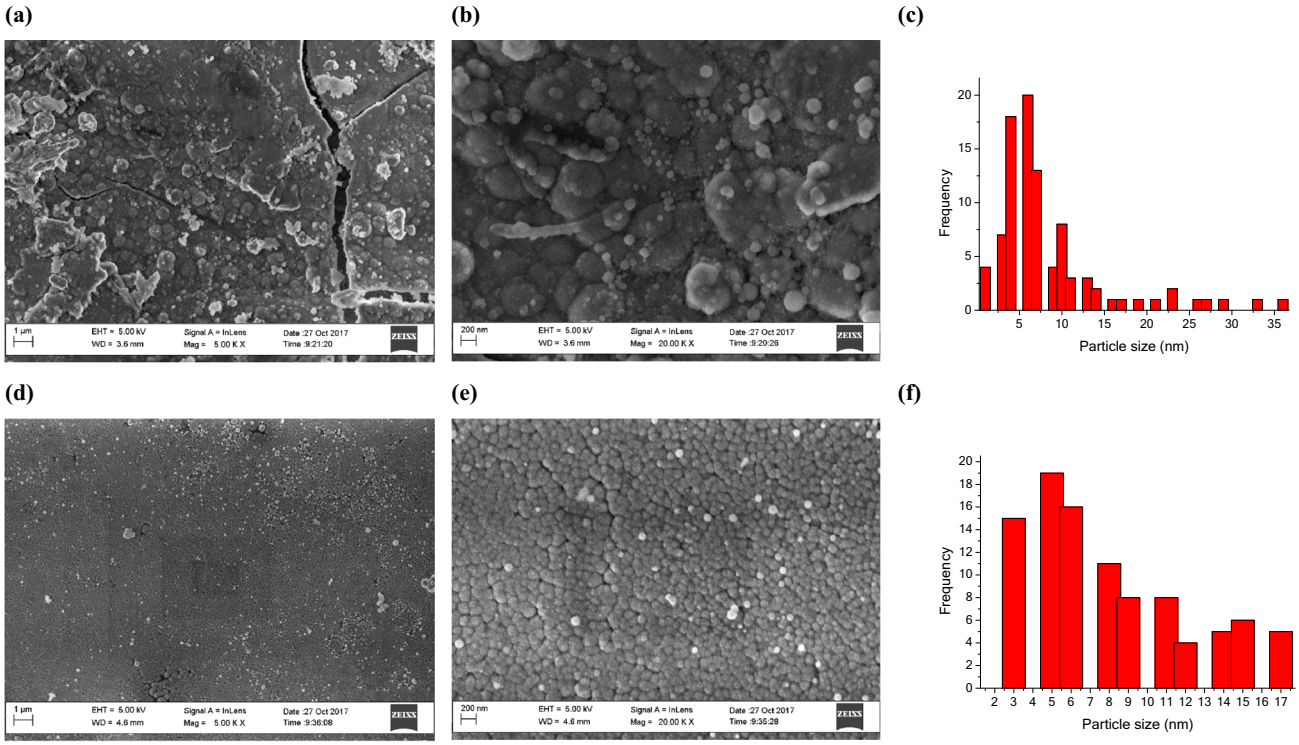


**Figure 3.** SEM micrographs of (**a**, **b**) Pd-$LaNi_5$ and (**c**, **d**) Pd-$LaNi_{4.8}Sn_{0.2}$ samples and their particle size distribution histograms ((**c**) Pd-$LaNi_5$ and (**f**) Pd-$LaNi_{4.8}Sn_{0.2}$).

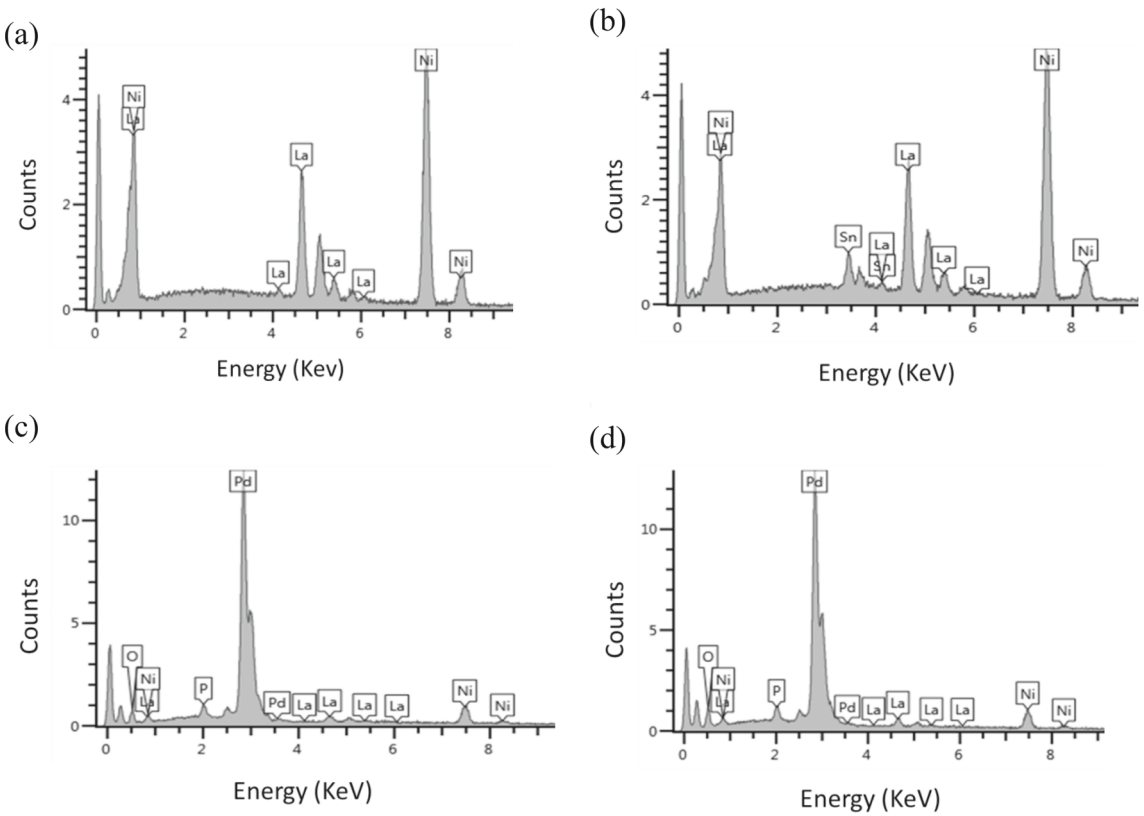


**Figure 4.** EDS plots of (**a**) $LaNi_5$, (**b**) $LaNi_{4.8}Sn_{0.2}$, (**c**) Pd-$LaNi_5$ and (**d**) Pd-$LaNi_{4.8}Sn_{0.2}$.

### 3.3 *Gas absorption studies*

3.3a *Nitrogen adsorption–desorption isotherms:* BET was used in this study to evaluate the effect of metal substitution (Sn for Ni) and autocatalytic deposition of Pd on the physisorption properties (surface area, pore volume and pore size) of the $AB_5$ materials (figure 5). The analysis was performed by the flow of the nitrogen on the materials. Figure 5a–d shows the nitrogen adsorption and desorption by all materials. None of the four isotherms exhibits hysteresis behaviour. The nitrogen adsorption and desorption isotherms of the unmodified alloys may be classified as type 1 isotherm group, due to the hump-shaped curve occurring at relative pressure of 0.3, while the straightened isotherms of Pd-coated alloys can be categorized as type 2 isotherm group [26]. The intermediate flat region observed with isotherms of Pd-modified materials resembles the monolayer formation. On an average, the uncoated alloys absorbed the lowest maximum nitrogen quantity of 0.6 $cm^3\ g^{-1}$ (figure 5). They were followed by Pd-coated $LaNi_{4.8}Sn_{0.2}$ alloy, which absorbed 2.558 $cm^3\ g^{-1}$ of nitrogen gas. Pd-coated $LaNi_5$ alloy absorbed the largest nitrogen gas (11.39 $cm^3\ g^{-1}$).

In figure 5, it is observed that the BET surface area of $LaNi_5$ is 0.1889 $m^2\ g^{-1}$, which is close to the reported one of 0.25 $m^2\ g^{-1}$ by Forde *et al* [27]. The surface area of the alloy was reduced to 0.1770 $m^2\ g^{-1}$ after Sn-substitution. The figure further indicates that the surface areas of the two unmodified materials were further decreased by autocatalytic deposition of palladium. The observed decrease in surface area after palladium deposition could be attributed to an increase in the metal loading on the surface of the materials [15].

3.3b *Hydrogen absorption kinetics:* The equilibrium hydrogen absorption/desorption performances, pressure-composition temperature (PCT diagrams) play an important role in determining the thermodynamic properties of metal hydride alloys as well as to understand the hydrogen absorption kinetics [4,8]. The PCT data of the $LaNi_5$ and $LaNi_{4.8}Sn_{0.2}$ materials were reported by Kodama [28] and Dehouche *et al* [29] to reveal the thermodynamic properties. The values of entropy ($\Delta S^0$) and enthalpy ($\Delta H^0$) for $LaNi_5$ material were reported to be $-110.0$ J $(mol\ H_2\ K)^{-1}$ and $-31.80$ kJ $mol^{-1}$ $H_2$ [28], whereas $LaNi_{4.8}Sn_{0.2}$ material has the $\Delta S^0$ and $\Delta H^0$ values of

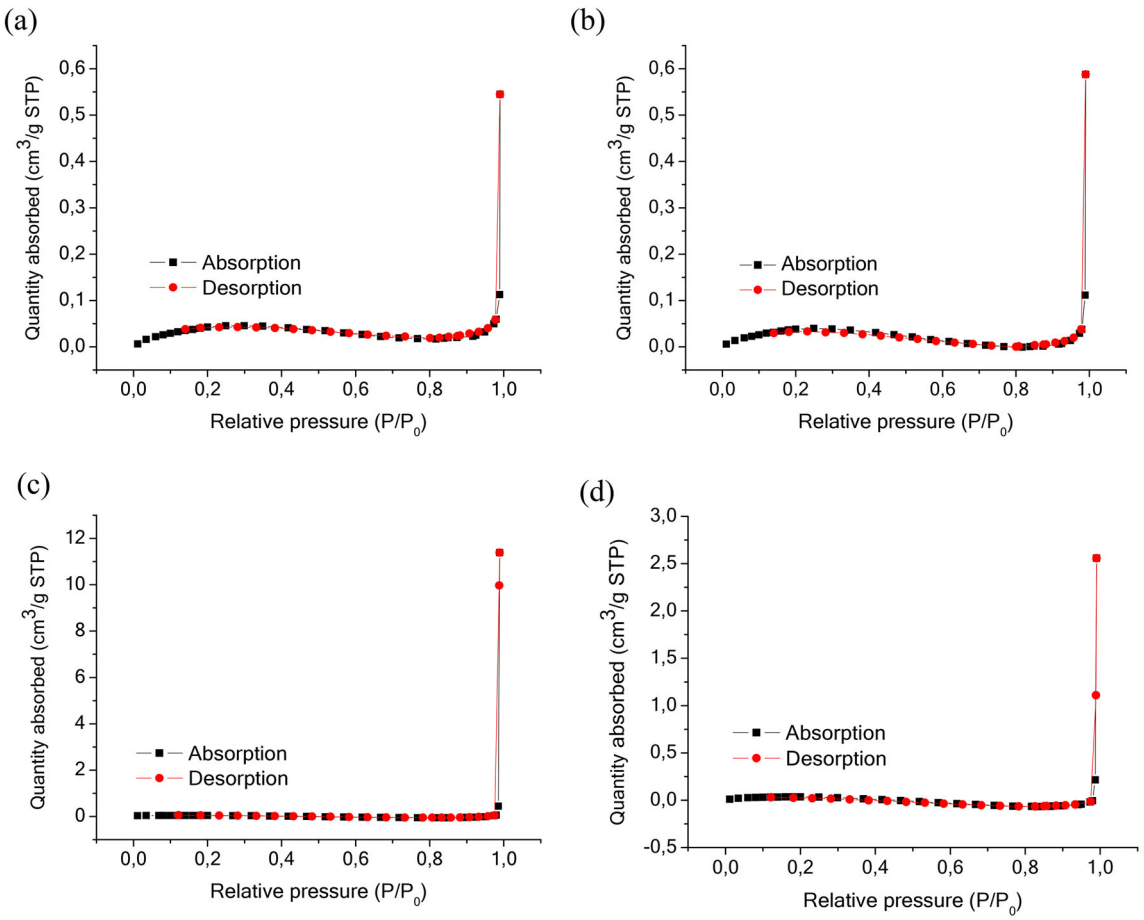


**Figure 5.** Adsorption–desorption isotherm of BET for (**a**) $LaNi_5$, (**b**) $LaNi_{4.8}Sn_{0.2}$, (**c**) Pd-$LaNi_5$ and (**d**) Pd-$LaNi_{4.8}Sn_{0.2}$.

$-104.3$ J (mol $H_2$ K)$^{-1}$ and $-32.83$ kJ mol$^{-1}$ $H_2$ [29]. Hydrogen absorption kinetics of non-activated and of activated samples were studied using hydrogen absorption experiments on a Sieverts-type volumetric setup, which were tested at 30 bar initial hydrogen pressure and constant temperature of 20°C. The materials were divided into two groups. The first group included the non-activated unmodified and modified materials and is presented in figure 6. As depicted by the figure, both unmodified alloys exhibited very long incubation periods before hydrogen absorption can take place. This observation can be attributed to the fact that during exposure to air, the materials allowed surface oxidations to take place, readily forming oxides film that prevents hydrogen dissociation and penetration into the interstitial sites [26,27]. The partial substitution of Sn for Ni resulted in an increase in maximum hydrogen storage capacity. The presence of protective surface oxide layers on the surfaces of the alloys is further suggested by sigmoid-shaped kinetic curves of these alloys [26]. Leon [26] further advised that the shape of these kinetic curves is a characteristic of a nucleation process. The index of power $n$ (obtained using equation (1)) for unmodified $LaNi_5$ and $LaNi_{4.8}Sn_{0.2}$ alloys were found to be 0.99 and 0.50, respectively (table 3). This indicates that the hydrogen absorption reaction for $LaNi_5$ alloy is controlled by nucleation and diffusion, while for $LaNi4_{.8}Sn_{0.2}$ alloy only the diffusion mechanism is involved according to Forde *et al* [27]. Therefore, the rate limiting steps for the unmodified alloys are surface processes together with nucleation and diffusion mechanisms.

On the other hand, Pd-coated $LaNi_5$ alloy exhibited an incubation period of less than 2 min before hydrogen absorption could take place, but a sigmoidal curve was still maintained by this alloy. Pd-coated $LaNi_{4.8}Sn_{0.2}$ alloy showed superiority over the other three alloys in terms of hydrogen absorption rate, with its kinetic curve revealing no presence of incubation period. This observation shows the importance of combining partial substitution of Sn for Ni and autocatalytic Pd deposition methods. It is well documented that Pd acts as a catalyst for hydrogen molecules splitting and transfer into the bulk alloy, consequently, and improving initial activation [30]. Moreover, Liu [31] reported that alloys with amorphous surfaces absorb hydrogen faster compared to their crystalline counterparts. It was seen that amorphous phosphorus particles from the electroless plating bath facilitated the creation of an interfacial channel between the bulk alloy and the palladium surface [20]. This may have increased the rate of transport of the hydrogen atoms, after dissociation of the hydrogen molecules on the palladium particles, and towards the bulk material. Hydrogen absorption reactions for both Pd-coated alloys are controlled by nucleation and diffusion mechanisms as suggested by their index of power (table 3).

The second group included unmodified and modified materials, which were activated prior to measurement of hydrogen absorption for 1 h under vacuum heating at 300°C), the materials were then cooled to ambient temperature (20°C), followed by $H_2$ absorption. The $H_2$ absorption kinetic curves are presented in figure 7. The

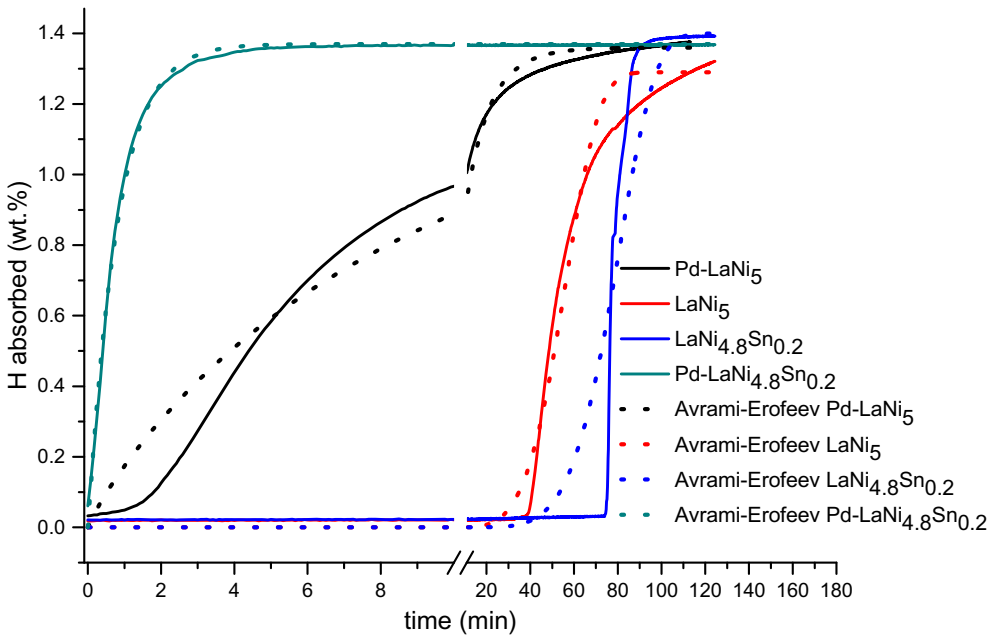


**Figure 6.** Dynamics of hydrogen absorption ($T$ = 20°C, $P_{H2}$ = 30 bar) by uncoated and Pd-coated $AB_5$ alloys after pre-exposure to air and no preliminary activation (no vacuum heating, solid and dash lines are experimental and fitted data, respectively).

**Table 3.** Fit of the experimental data for hydrogen absorption by non-activated and activated materials using the Avrami–Erofeev equation.

| Sample | $\left(\frac{H}{AB5}\right)_{max}$(wt%) | | Rate constant, k ($min^{-1}$) | | Index of power | |
|---|---|---|---|---|---|---|
| | Non-activated | Activated | Non-activated | Activated | Non-activated | Activated |
| $LaNi_5$ | 1.29 | 1.45 | 0.06 | 0.21 | 0.99 | 0.98 |
| $LaNi_{4.8}Sn_{0.2}$ | 1.40 | 1.37 | 0.24 | 19.21 | 0.50 | 0.58 |
| Pd-$LaNi_5$ | 1.36 | 1.47 | 0.16 | 7.04 | 0.62 | 0.68 |
| Pd-$LaNi_{4.8}Sn_{0.2}$ | 1.37 | 1.35 | 1.32 | 68.03 | 0.97 | 0.50 |

kinetic curve of $LaNi_5$ material shows improvement in both the absorption kinetics and maximum hydrogen uptake capacity with a reduced incubation period, suggesting that the oxide film was removed through vacuum heating. However, the sigmoid shape is still present; suggesting that the oxide film was not completely removed or initial activation of the alloy is generally poor. The index of power for this particular alloy slightly dropped from 0.99 to 0.98, signifying that nucleation and diffusion mechanisms are still the dominant rate determining steps during hydrogen absorption reaction. The maximum hydrogen absorbed and rate constant of $LaNi_5$ alloy were enhanced from 1.29 to 1.45 wt% and from 0.06 to 0.21 $min^{-1}$, respectively (table 3). There was noticeably a small decrease in hydrogen capacity upon Sn substitution. This was attributed to the formation of slightly amorphous phase, as it can be seen when comparing X-ray pattern of $LaNi_5$ with that of $LaNi_{4.8}Sn_{0.2}$ in figure 1a and b. Furthermore, the substitution of nickel by Sn changes some properties of the $LaNi_5$ alloy, the substitution leads to a significant decrease in the degradation of the alloy [32]. This improves its cycling stability in thermal cycling in hydrogen and in an electrochemical cell [33]. However, the cell parameters increase with Sn substitution in LaNi5, due to the replacement of nickel (RNi = 1.24 Å) by a larger atom (RSn = 1.62 Å). Due to the difference in size, the substitution leads to an increase in the cell volume, which in turn leads to a marginal decrease in hydrogen storage capacity [34]. The kinetic curves of $LaNi_{4.8}Sn_{0.2}$, Pd-$LaNi_5$ and Pd-$LaNi_{4.8}Sn_{0.2}$ alloys exhibited similar

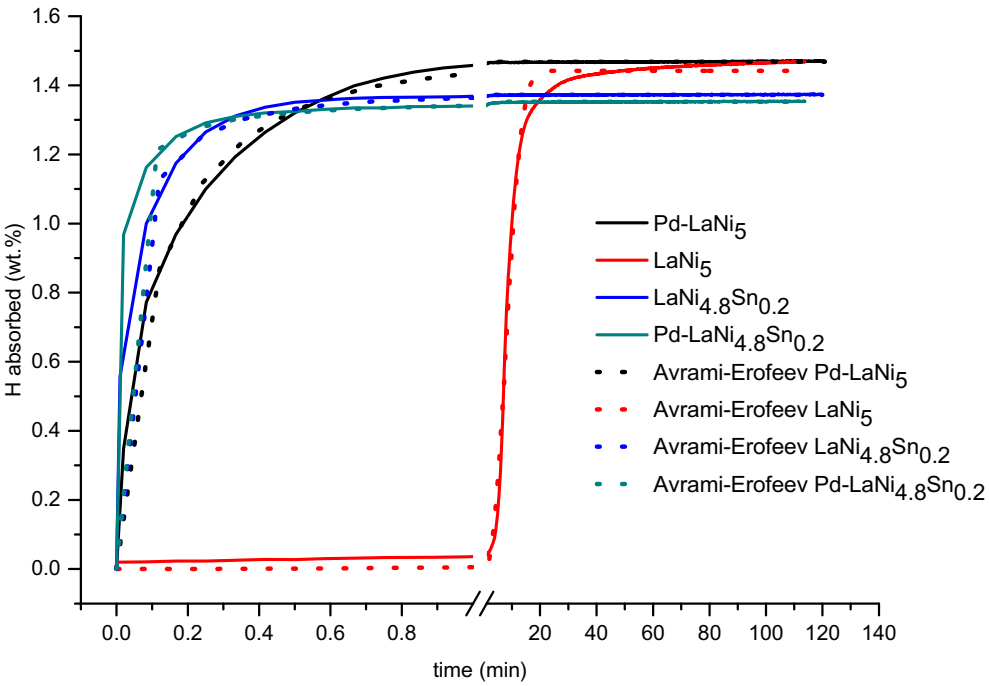


**Figure 7.** Dynamics of hydrogen absorption ($T$ = 20°C, $P_{H2}$ = 30 bar) by uncoated and Pd-coated $AB_5$ alloys after preliminary activation (vacuum heating at 300°C, solid and dash lines are experimental and fitted data, respectively).

trend with no or little incubation period, in comparison with the first non-activated group due to a complete removal of oxide film, leading to an oxide-free metal surface as observed by Shan and co-workers [35]. Table 3 depicts that the power index of Pd-coated $LaNi_{4.8}Sn_{0.2}$ alloy is the only one that changed significantly after activation from 0.97 to 0.50. This observation implicates that once the alloy is activated, nucleation mechanism is no longer playing a role as rate determining step during hydrogen absorption process. The supremacy of Pd-coated $LaNi_{4.8}Sn_{0.2}$ alloy over the other alloys is still depicted by its kinetic curve, reaching maximum hydrogen capacity within 0.2 min with a highest rate constant of 68.03 $min^{-1}$ (table 3).

## 4. Conclusion

The experimental study herein presented the effect of combining Sn-substitution and electroless Pd deposition on the hydrogen absorption kinetics of $LaNi_5$ alloy. The study shows that Sn-substitution alone does not significantly improve the poisoning tolerance of the parent material, as shown by sigmoid-shaped kinetic curve of the non-activated $LaNi_{4.8}Sn_{0.2}$ alloy and long incubation period. Interestingly, the alloy benefited from Sn-substitution since a slight enhancement of maximum hydrogen storage capacity by 0.11 wt% after exposure to air was observed. This small change in hydrogen storage capacity can be attributed to an increase in the unit cell volume observed from XRD results. All materials (non-activated and activated) that underwent autocatalytic deposition of palladium showed excellent $H_2$ absorption kinetics. It is therefore deduced that Pd layer on the surface of the materials is able to prevent the formation of oxides, promoting fast absorption of hydrogen by reducing the incubation period. Furthermore, the impregnation of phosphorus-containing electroless plating bath, which is amorphous in nature, may have also played a role in enhancing the hydriding kinetics by creating an interfacial channel between the bulk alloy and the palladium surface. We also noticed that Sn-substitution materials have hydrogen uptake capacity of ca. 10% lower than those of non-substituted materials.

## Acknowledgement

KDM and MJH would like to thank the National Research Foundation (Grant nos. 118113 and 117984), University of Limpopo (Research Development Grants R202 and R232), South Africa, for financial support. We are also grateful to the Sasol Inzalo Foundation of South Africa for procurement of the STA instrument.

## References

[1] Kato S, Matam S K and Rohwerder M 2016 *Angew. Chem. Int. Ed.* **55** 6028
[2] Gahleitner G 2012 *Int. J. Hydrog. Energy* **38** 2039
[3] Somo T R, Mabokela T E, Teffu D M, Sekgobela T K, Hato M J and Modibane K D 2021 *Chem. Pap.* **15** 1
[4] Williams M, Lototsky M, Nechaev A, Yartys V, Solberg J K, Denys R V *et al* 2010 *Afr. J. Anim. Sci.* **106** 1
[5] Chen Y, Sequeira C A C, Song X, Neto R and Wang Q 2002 *Int. J. Hydrog. Energy* **27** 63
[6] Schlapbach L and Züttel A 2011 in V Dusastre (ed) *Materials for sustainable energy* (Singapore: Springer Nature Publishing Group) p 265
[7] Zhang D Z Y, Li B, Ren H, Li X and Qi T 2011 *Materials* **4** 274
[8] Modibane K D, Williams M, Lototskyy M V, Davids M W, Klochko Y and Pollet B G 2013 *Int. J. Hydrog. Energy* **38** 9800
[9] Liu J, Song X P and Chen G L 2009 *J. Alloys Compd.* **486** 338
[10] Somo T R, Maponya T C, Davids M W, Hato M J, Lototskyy M V and Modibane K D 2020 *Metals* **10** 562
[11] Zhang Y, Zhang W and Qi W B Y 2017 *Acta Metall. Sin.* **30** 1040
[12] Kyoi D, Sakai T, Kitamura N, Ueda A and Tanase S 2008 *J. Alloys Compd.* **463** 306
[13] Souza E C and Ticianelli E A 2003 *J. Braz. Chem. Soc.* **14** 544
[14] Cuevas F and Hirscher M 2000 *J. Alloys Compd.* **313** 269
[15] Alshaibani A 2017 *Arab. J. Chem.* **10** 1188
[16] Zhang Y, Xu S and Zhao D 2014 *Trans. Nonferrous Met. Soc. China* **24** 3524
[17] Modibane K D, Lototskyy M V, Davids M W, Williams M, Hato M J and Molapo K M 2018 *J. Alloys Compd.* **750** 523
[18] Yeung K L, Christiansen S C and Varma A 1999 *J. Memb. Sci.* **159** 107
[19] Hubkowska K, Soszko M and Czerwiński A 2019 *Electrochem. Commun.* **100** 100
[20] Denys R V, Lototskyy M V, Linkov V M and Williams M 2010 *S. Afr. J. Sci.* **106** 9
[21] Lototskyy M V, Modibane K D, Williams M, Klochko Y, Linkov V M and Pollet B G 2013 *J. Alloys Compd.* **580** 382
[22] Willey D B, Pederzolli D and Harris I R 2002 *J. Alloys Compd.* **332** 806
[23] Ishibashi Y, Terashima M and Yamakawa R 2005 *J. Alloys Compd.* **402** 219
[24] Anthuvan J, Pandurangan A and Senthil C 2014 *Mater. Res. Bull.* **60** 621
[25] Kumar R, Joardar J and Raman S 2017 *Materials* **10** 272
[26] Leon A 2002 *J. Alloys Compd.* **345** 158
[27] Forde T, Maehlen J P, Yartys V A, Lototsky M V and Uchida H 2007 *Int. J. Hydrog. Energy* **32** 1041
[28] Kodama T 1999 *J. Alloys Compd.* **289** 207
[29] Dehouche Z, Grimard N, Laurencelle F, Goyette J and Bose T K 2005 *J. Alloys Compd.* **399** 224
[30] Parambhath V B, Nagar R and Ramaprabhu S 2012 *Langmuir* **28** 7826

[31] Liu F J 1995 *J. Alloys Compd.* **231** 696
[32] Beeri O, Cohen D, Gavra Z, Johnson J R and Mintz M H 1992 *J. Alloys Compd.* **113** 187
[33] Khyzhun O, Lototsky M V, Riabov A B, Rosenkilde C, Yartys V A, Jørgensen S *et al* 2003 *J. Alloys Compd.* **356** 773
[34] Joubert J M, Latroche M, Cerny R, Bowman R C Jr, Percheron-Guegan A and Yvon K 1999 *J. Alloys Compd.* **124** 293
[35] Al L, Ni M, Shan X, Payer J H and Wainright J S 2006 *J. Alloys Compd.* **426** 400